

ORIGINAL RESEARCH

## Placing sensors optimally in base-isolated steel structures using a multi-objective optimization approach

Firoozbakht M.<sup>1</sup>, Vosoughifar H.<sup>2,\*</sup>, Ghari Ghoran A.<sup>3</sup>


### Abstract:

Adequate selection of sensors placement plays a key role in structural health monitoring (SHM) in base isolated (BI) structures. This critical issue is usually done by past experience and knowledge on the force and vibration situations of a structure. During recent decades, techniques have received increasing attention as a tool for determining an arrangement of sensors suitable for SHM. In this paper, a multi-objective numerical method for optimal sensor placement (OSP) in BI structures based on the combination of traditional OSP algorithms and nonlinear time-history analysis (NTH) has been proposed. Next, genetic algorithm (GA) was employed to determine the location of sensors on the structure based on the structural dynamic response of the BI system. To show the efficiency of the proposed method, a BI building was modeled using finite element method (FEM) in which NTH were undertaken using the seismic scaled records of near-fault earthquakes (NF). The novel numerical approach called transformed time history to frequency domain (TTFD) was evaluated to transform NTH results to frequency domain and then the effective frequencies according the maximum range of Fourier amplitude were selected. The modified type of modal assurance criteria (MAC) values can be achieved from MAC with the exact seismic displacement. Results show that the proposed method can provide the optimal sensor locations and remarkably reduce the number of required sensors and also improve their optimum location.

### Keywords:

Structural Health Monitoring (SHM), Optimal Sensor Placement (OSP), Base Isolated (BI) structures, Nonlinear Time-History Analysis (NTH), Genetic Algorithm (GA), Transformed Time history to Frequency Domain (TTFD)

---

\*Corresponding author Email: hmvosoughifar@gmail.com

1 Department of Civil Engineering, Isfahan (Khorasgan) Branch, Islamic Azad University, Isfahan, Iran

2 Department of Civil and Environment, Hawaii University at Mano, Hawaii, USA (Vosoughi@Hawaii.edu)

3 Department of Civil and Transportation Engineering, Isfahan University, Isfahan, Iran

## 1. Introduction

The smart sensors, remote sensing, and decision making knowledge are used in SHM process to monitor and damage detection of structures. It is well known that for SHM, many sensors have to be installed at various points of a structure. Due to practical reasons such as the inaccessibility of some degrees of freedom, or owing to economic factors concerning the cost related to instrumentation and data analysis, responses are generally recorded in a the number of locations which is smaller than the total number of degrees of freedom of the structure. Optimally configuration can minimize the number of sensors, increase accuracy and provides the best observability and controllability to identify the target modes for solving the above problem. The various techniques for OSP based on behavior of structure and cost-minimization were developed. Hence, since damage is always accompanied by a reduction of stiffness as well as modal frequency, calculating the change of modal frequency has been widely applied in damage alarming. Nevertheless, it remains difficult to distinguish the damage location just by this trait. Among the modal analysis (MA) parameters of a structural system, the mode shape is obviously the only location related parameter [1]. Therefore, many researchers have attempted to establish mode shape based indicators, such as the MAC [2-3] and coordinate modal assurance criterion (COMAC) indexes [4] to identify damage and its locations. However, it has been shown that they have low sensitivity to damage in some cases [5-6]. By extending these ideas, the MinMAC algorithm [7] was proposed to overcome existing problems with using the contra decreasing approach. Then, a forward-backward combinational extension [8] was developed. Another approach based on maximization of the determinant of the Fisher information matrix called the effective independence (EI) [9-10] was utilized for the structural modal identification and optimization. Placing the sensors in locations with low energy content is the most important

restriction of the recent method. This approach is modified by considering driving point residue (DPR) coefficient [11-12]. In other similar method that called kinetic energy (KE) optimization [13], the amount of KE is measured instead of the Fisher's data matrix. Some similar methods, e.g. the maximum eigenvalue vector product (EVP) [14] and mode shape summation Plot (MSSP) [15] were used through finding the maximum EVP and MSSP values. These calculations were done in order to prevent the placement of sensors on nodal lines. A different approach consists in minimizing the information entropy [16]; measuring the uncertainty in the system parameters was introduced to make comparisons between sensor configurations involving a different number of sensors in each figuration. The methodology has also been extended in [17] to design sensor locations for updating multiple model classes useful for damage detection purposes. Another different methodology also calculates unknown responses in locations where sensors are not available using a spline shape function to interpolate record response along the height of the building [18].

In this research, the OSP procedure of BI structures subjected to NF earthquakes is studied using a novel approach. For this purpose, a BI structure was modeled using FEM in which NTH were undertaken using the seismic scaled records of NF earthquakes. Furthermore, three various OSP algorithms were used and GA was selected to act as the solution of the optimization formulation.

## 2. Description of the proposed method

The main purpose of evaluating a novel approach is to develop the existing MAC criteria with worthier computational process and make more reliable method in this issue. The existing MAC method is used for initial placement of the sensors set, based on the maximum values of the off diagonal Mac elements, leading to the selection of to modes with high similarity. In other words, the use of MAC in target structures is performed with

the aim of creating the sensors layout at locations with higher values of displacements in the combination of modes. In fact, locations with highest displacement in the combination of modes are utilized for sensor placement. After forming the MAC matrix, modes with a particular MAC value are considered, and modal displacement is calculated using the root mean square of values. Hence, the displacement of a node in the first mode with the same displacement of the node in the second mode is combined. Such work is performed for all nodes, and its values are stored in a matrix. Then, the nodes with the maximum combined displacement are selected as the initial location of sensors. Moreover, the corresponding MAC values are considered as a term in the forming of the objective function. It should be noted that the duplicated values are detected and deleted.

The novel numerical approach called Transformed Time History to Frequency Domain (TTFD) was evaluated to transform NTH results to frequency domain and then the effective frequencies according the maximum range of Fourier amplitude were selected. This novel criterion was carried out using NTH to make modified type of MAC method and estimate the OSP. Because the BI steel structures have effective natural modes, the modified-MAC values of the seismic waves corresponding each level were calculated. The frequency domain obtained with the FEM-MAC-TTFD criteria was used to analysis the NF seismic waves in OSP process. This approach can consider the actual earthquake waves on MAC algorithm. The basic idea is applied to generate frequency amplitude from displacement that obtained from time history analysis. Finally, the GA is adopted to determine the final locations of the sensors. Overall, the proposed methodology can optimize the number and placement of sensors for SHM of BI steel structures subjected to seismic loads.

### 3. Modeling Structural molding description

In the present study, an actual three-dimensional (3D) steel building, with one

Lead Rubber Bearing (LRB) seismic isolation device under each column, has been investigated. The considered building is used as a school located at the high damage risk zone. Therefore, health monitoring of this structure is plausible. The aforementioned building is an actual 5-story steel building with an irregular plan, and the Load Resistance Factor Design (LRFD) algorithm was used for the design procedure based on the American Institute of Steel Construction (AISC) code [19]. This building is equipped with a total number of 67 LRBs in its isolation base under each column. A 3D view of the FE model is depicted in Figure 1.

The most common base isolation devices used over many years by engineers are LRB isolators which combine isolation function and energy dissipation in a single compact unit [20-21]. Such LRB isolator devices provide vertical load support, horizontal flexibility, supplemental damping, and centering force to the structure from earthquake attack. In addition, they require minimal cost for installation and maintenance as compared to other passive vibration control devices [22-23]. The LRB isolator is composed of an elastomeric bearing made by laminated rubber layers with steel shim plates, cover plates, and a lead core located on its center. The typical LRB isolator device is shown in Figure 2. The typical LRB isolator has considerable maximum shear strains corresponding to between 125% and 200% because reinforcing steel plates have little effect on the shear stiffness. This LRB isolator device can combine the function of isolation and recentering in a single unit (*i.e.*, elastomeric bearing), thereby giving structural support, horizontal flexibility, and recentering force to the isolation system [24-25]. Furthermore, it produces the required amount of supplemental damping and energy dissipation by adjusting the size of the lead core. The energy dissipation generated by the yielding of the lead core achieves an equivalent viscous damping coefficient up to approximately 30%, and effectively reduces the horizontal displacement. The LRB isolators are usually fabricated in circular sections, and sometimes

produced with more than one lead core. A LRB model practically used in the construction field is selected in this study. Including geometric details illustrated in Figure 2, mechanical properties needed to simulate their force-displacement responses are presented in Table 1. As shown in Figure 3, the force-displacement responses can be ideally modeled as bilinear hysteresis loops.

The bilinear hysteresis loops considered herein are defined as four key parameters given in Table 1 per each LRB model, such that: yield displacement ( $\Delta 1$ ), yield force ( $F1$ ), specified design displacement ( $\Delta 2$ ), and its corresponding force ( $F2$ ). The elastic stiffness ( $Ke$ ) and the post-yield stiffness ( $Kp$ ) are defined as Equations (1) and (2).

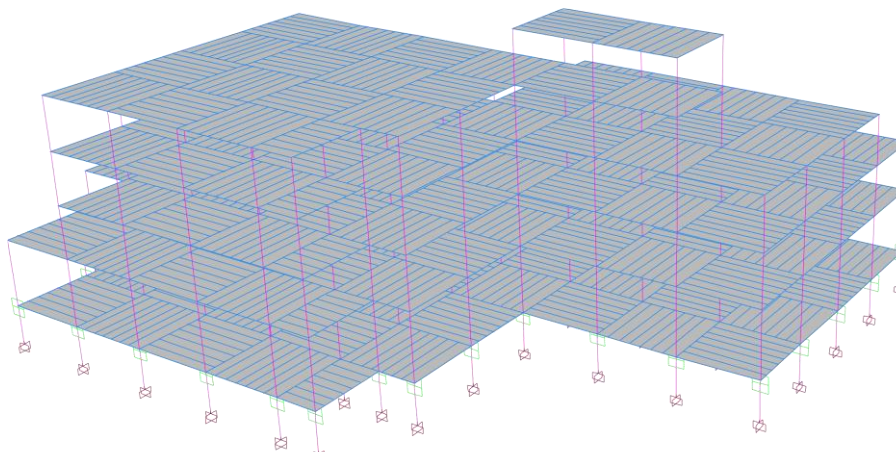


Fig. 1. The 3D view of FE structural model

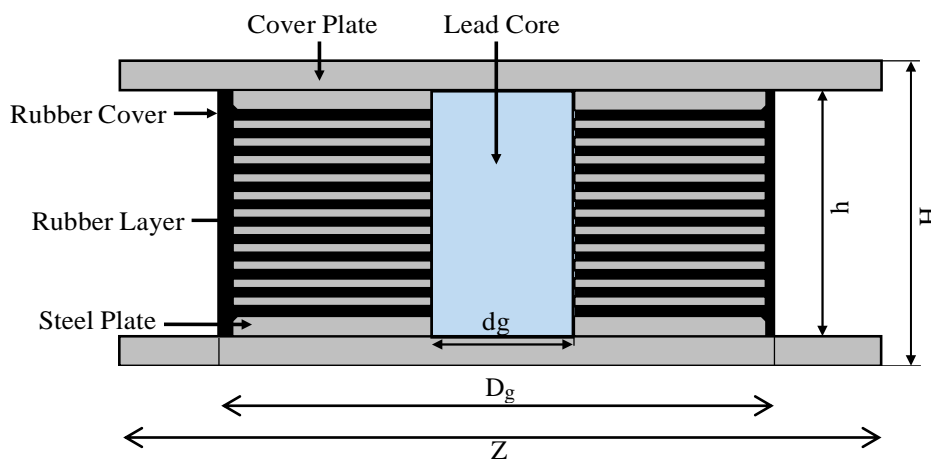


Fig. 2. Typical LRB isolator device

Table 1. Properties of the LRB isolator model

characteristic	$\Delta m_x$	$F_v$	$F1$	$F2$	$\Delta 1$	$\Delta 2$	$Q$	$Ke$	$Kp$	$Ke_{eff}$	$\lambda_{eff}$	$Z$	$D_g$	$d_g$	$H$	$h$	$te^*$
Unit	mm	kN	kN	kN	m	m	kN	kN/m	kN/m	kN/m	mm	m	m	m	m	m	m
Value	400	3170	259	651	16	333	239	16.19	1.24	1.95	22.3%	800	750	170	397	337	203

\* Total thickness of the rubber

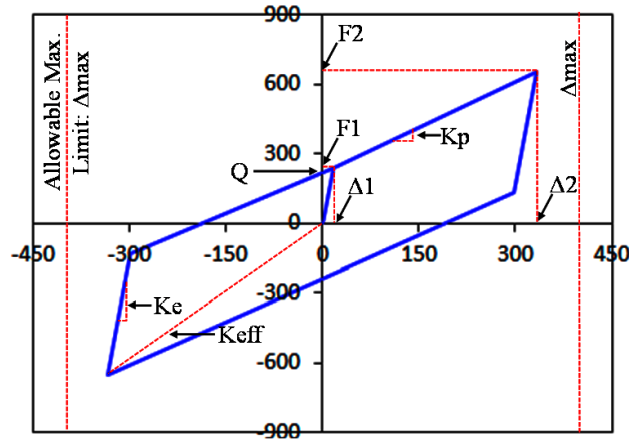


Fig. 3. Hysteresis loop of the presented LRB isolator device modeled as bilinear curves

$$(1) K_e = \frac{F1}{\Delta1}$$

$$(2) K_p = \frac{F2 - F1}{\Delta2 - \Delta1}$$

The effective stiffness of the hysteretic behavior ( $K_{eff}$ ) can be modeled the secant line by means of the ratio as Eq. (3).

$$(3) K_{eff} = \frac{F2}{\Delta2}$$

The characteristic strength indicating force-intercept at the zero displacement ( $Q$ ) can be also expressed as the function of the post-yield stiffness as Eq. (4).

$$(4) Q = F1 - K_p \cdot \Delta1$$

The hysteretic loop area ( $E_{iso}$ ) representing the amount of energy dissipation can be obtained from Eq. (5).

$$(5) E_{iso} = 4Q \cdot (\Delta2 - \Delta1)$$

The effective viscous damping coefficient ( $\lambda_{eff}$ ) is proportional to the amount of energy dissipation, but inversely related to both the effective stiffness and the square displacement. This damping coefficient also depends on four key parameters, which it

refers:

$$(6) \lambda_{eff} = \frac{E_{iso}}{2\pi \cdot K_{eff} \cdot (\Delta2)^2} = \frac{2}{\pi} \left( \frac{F1}{F2} - \frac{\Delta1}{\Delta2} \right)$$

The mechanical properties obtained from calculations in the above equations are summarized in Table 1.

LRB has the maximum allowable horizontal displacement ( $\Delta_{max} = 400$  mm), representing 1.2 times the length of  $\Delta2$ .

#### 4. Verification

The verification of this novel approach was performed by statistical comparison between achieved results with Saiful Islam et al.'s [26] research on base isolation system. In this research a non-linear time domain analysis was also performed by choosing the proper ground motion that scaled with the site condition of Dhaka city in Bangladesh. The comparison between this study and Saiful Islam et al.'s research for top floor acceleration in X and Y direction with scatter plots are shown in Figure 4. There are good agreements between this study and the reference research ( $R^2=0.963$  in X direction and  $R^2=0.975$  in Y direction). In this regards, the novel approach has good accuracy to discretize governing equation for NTA.

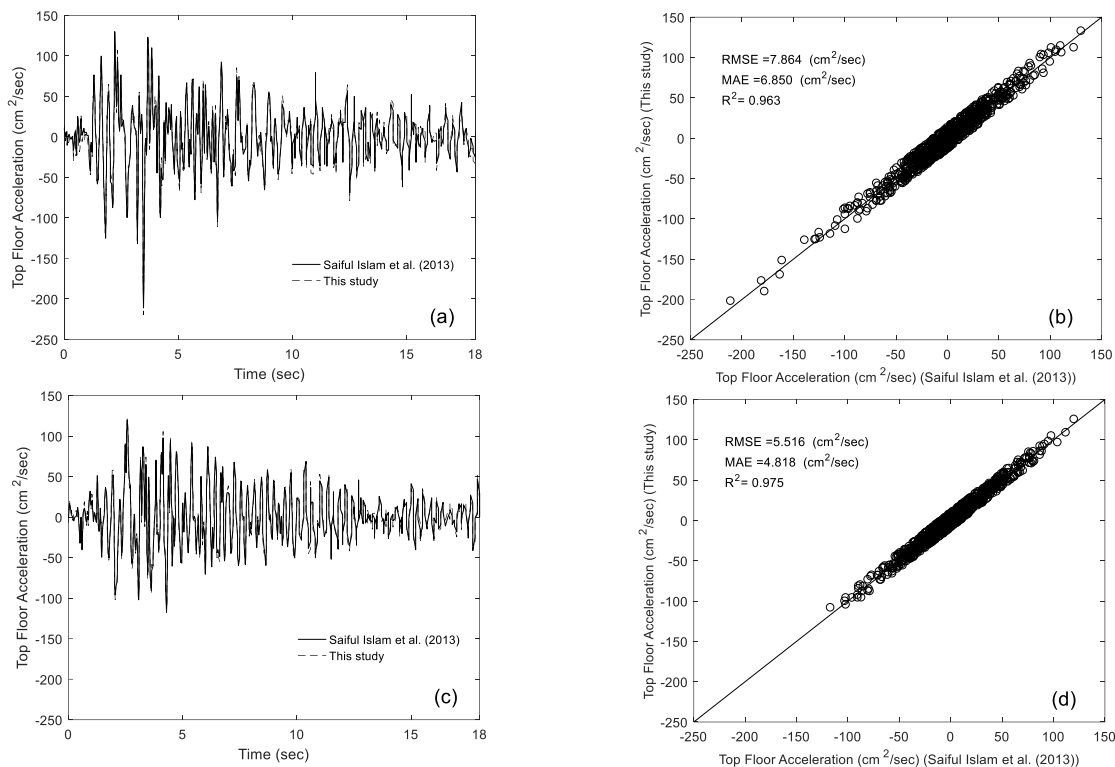


**Fig. 4. Top floor acceleration Time History, a) X direction, b) scatter plot in X direction, c) Y direction, d) scatter plot in Y direction**

## 5. Analysis Procedure

### 5-1- Modal analysis

Natural frequencies are the important characteristics of a structure. It can be used to analyze the results that obtained by dynamic analysis. The vibration properties were

calculated by performing MA. Table 2 presents the first six natural time periods and maximum modal responses of the proposed model. Figure 5 illustrates the first six mode shapes of the BI structure. It was often necessary to consider more fundamental modes in order to take account for 90% of the modal mass [27].

**Table 2. Modal analysis results; periods and maximum displacements**

Mode no.	Period (s)	Max Dis. (x cm)	Max Dis. (y cm)	Max Dis. (z cm)
1	4.01	0.037	0.039	0.03
2	3.89	0.036	0.038	0.029
3	3.26	0.03	0.033	0.026
4	1.07	0.019	0.026	0.017
5	1.04	0.018	0.025	0.015
6	0.919	0.016	0.023	0.014

### 5-2- Nonlinear time history analysis

One of the most important challenges in analyzing irregular structures is considering the effects of earthquakes on structural responses. Some scientists have raised special

concerns as to ordinary buildings that are vulnerable to strong impulsive NF ground motions [28-30]. The NF ground motions recording from recent earthquakes are different from general ground motions in that they contain a strong-narrow band pulse of

the spectral acceleration at short to intermediate periods [31-33]. Once ordinary frame buildings with relatively short vibration periods undergo these NF ground motions, inter-story drifts generated tend to be considerable due to strong ground acceleration pulses delivered into the column bases [34-37]. In this study, in order to select the appropriate earthquake records based on three criteria of magnitude, distance, and type of soil, the TOPSIS method is used [38]. Three sets of recorded earthquake ground motions

including NF seismic records were considered in NTH. The parameters of the selected ground motion records are given in Table 3. Responses of structure were obtained in  $x$ ,  $y$  and  $z$  directions. The evidences in Table 4 have been attained from dynamic analysis of the presented BI building. The time histories obtained are maximum base shear, base moment and displacements. As sample of performed analysis, Figure 6 illustrates the results of NTH under the Landers earthquake (1992).

**Table 3. The used seismic ground motion records**

Earthquake	Record ID	Magnitude ( $M_w$ )	PGA (g)	Site Classification
Landers (1992)	LADSP000	7.5	0.17	C
San Fernando (1971)	P0052	6.6	0.174	C
Northridge (1994)	NRORR360	6.8	0.51	C

**Table 4. Maximum results of nonlinear time-history analyses for a BI structure subjected to near-fault earthquakes**

Earthquake	Design base shear (kN) in $x$ direction	Design base shear (kN) in $y$ direction	Design base moment (kN-m) in $x$ direction	Design base moment (kN-m) in $y$ direction	Roof-story displacement (cm) in $x$ direction	Roof-story displacement (cm) in $y$ direction
Landers (1992)	2842	1956	38293	26228	7.98	7.89
San Fernando (1971)	2733	1869	37395	26004	7.01	6.68
Northridge (1994)	2779	1896	37786	26108	7.44	7.08

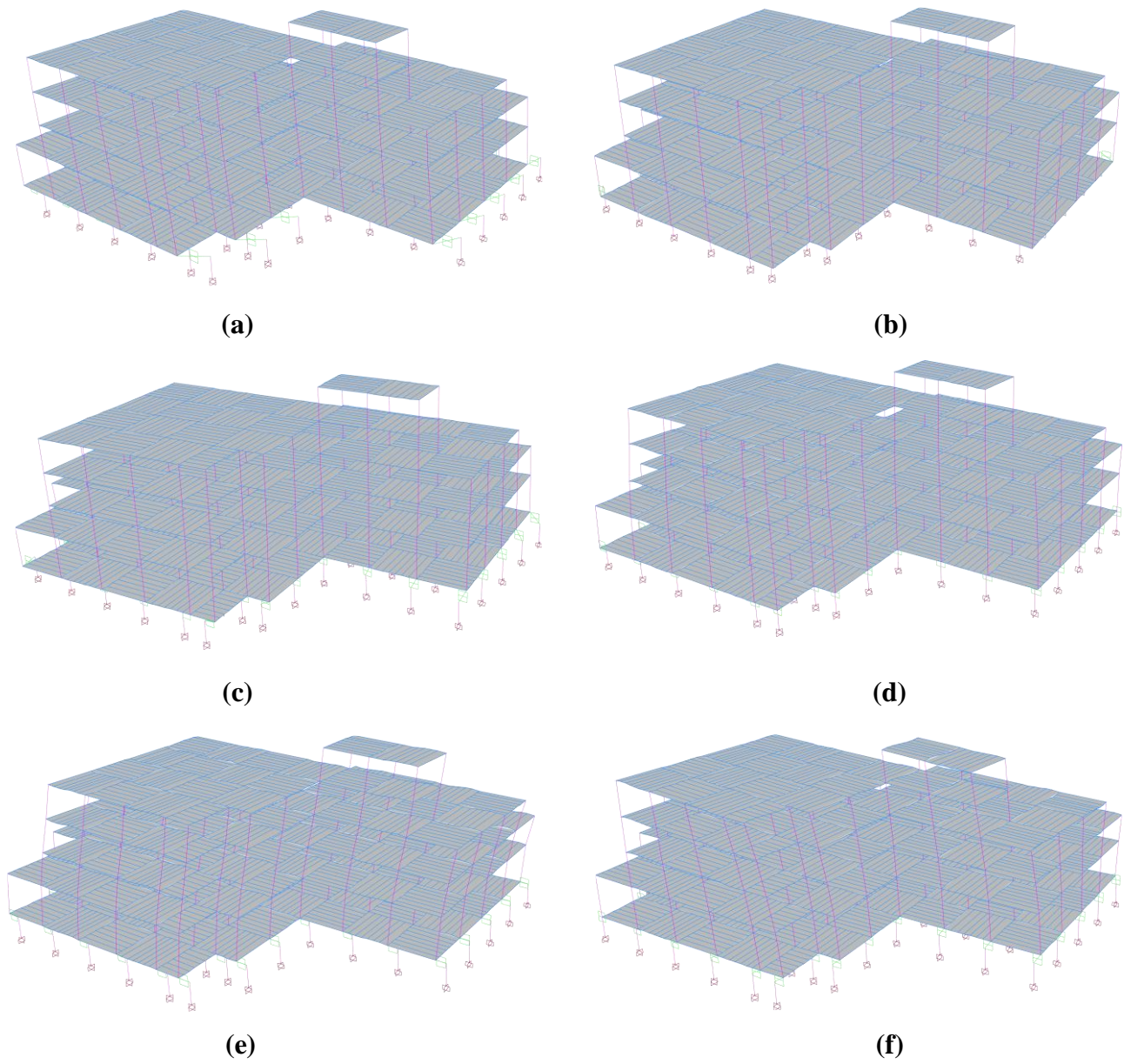


**Fig. 5. Mode shapes of BI structure (a) 1<sup>st</sup> (b) 2<sup>nd</sup> (c) 3<sup>rd</sup> (d) 4<sup>th</sup> (e) 5<sup>th</sup> (f) 6<sup>th</sup>**



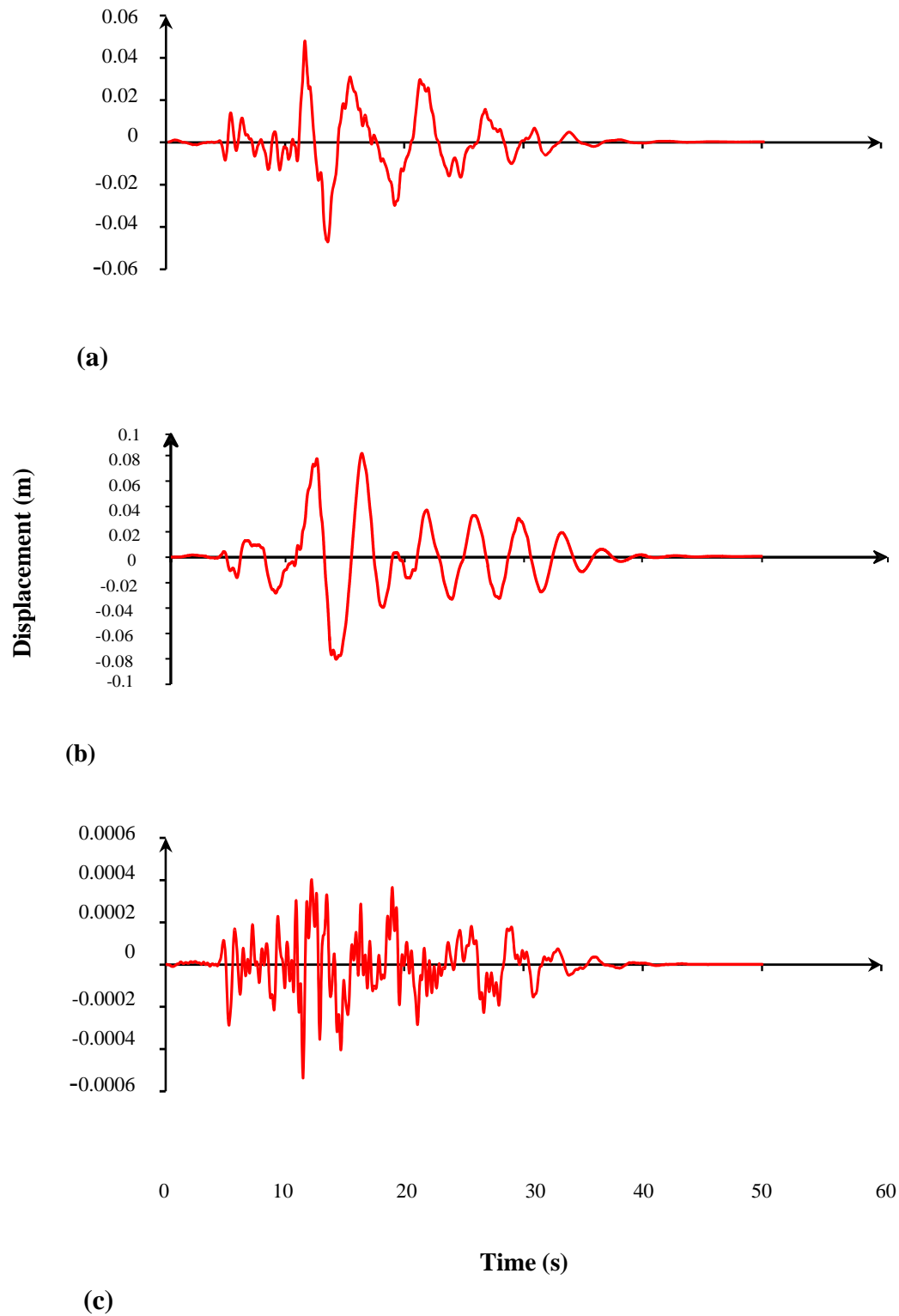


**Fig. 6. Displacement time-history of the BI systemsubjected to Landers earthquake (1992)  
(a: longitudinal, b: transverse, c: vertical components)**

## 6. Genetic Algorithm

To find the optimal solution of the objective function, the GA is used. The GA is well known due to its simplicity and robustness in the solution of complex problems so that these characteristics fit well to the problem described in this paper [39]. GAs have been widely used in sensor placement type problems [40].

The GA has been proved to be a powerful tool in the OSP; however, it has some faults that need to be rectified. For example, one sensor location may be placed where two or more sensors exist or sensor numbers are not equal to a certain number [41]. A good surveillance system must detect the aftermath of a contaminant spill as soon as possible with maximum reliability. Earlier detection gives more time to the system managers to react. Thus, an objective of the optimization is to maximize the detection time that can be defined in an average sense and an objective function.

In this optimization method, information about a problem, such as variable parameters, is coded into a genetic string known as a chromosome. Each of these chromosomes has an associated fitness value, which is usually determined by the objective function [42].

## 7. OSP process

Numerous techniques have been advanced for the OSP problem and were widely reported in the literature. These have been developed using a number of approaches and criteria, some are based on intuitive placement or heuristic approaches, and others may employ systematic optimization methods. The sensor placement optimization can be generalized as “given a set of  $n$  candidate locations, find the subset of  $m$  locations, where  $m \leq n$ , which may provide the best possible performance” [43].

As known, the measured mode shape vectors in the SHM have to be as possible linearly

independent, which is a basic requirement to distinguish, measured or identified modes. In this research, three different OSP algorithms are utilized which include MAC, extended MAC (EMAC) and TTFD.

### 7-1- MAC approach

All the past studies have been developed based on intuitive placement, heuristic approaches, and systematic optimization methods. The MAC is a mathematical criterion to check the compatibility between two eigenvectors. MAC matrix is defined as Eq. (7) [2-3].

$$(7) \text{MAC}_{ij} = \frac{(\phi_i^T \phi_j)^2}{(\phi_i^T \phi_i)(\phi_j^T \phi_j)}$$

Where  $\phi_i$  and  $\phi_j$  represent the  $i$ th and  $j$ th column vectors in matrix  $\phi$ , respectively, and the superscript  $T$  denotes the transpose of the vector. In this equation, the MAC values fall within the range between 0 and 1. Zero value of MAC shows lack of any correlation between the off-diagonal element of matrix and one indicates a high degree of likeness between the modal vectors. Then, the maximum values of mode displacements for nodes corresponding to the maximum off-diagonal terms with Square-Root-of-Sum-of-Squares (SRSS) or Complete Quadratic Combination (CQC) were calculated. First, these points are selected for initial placement of sensors. Second, it adds other available candidate sensors one by one, and selects one that minimizes the maximum off-diagonal element of the MAC matrix at each step. Therefore, the MAC objective function is defined as Eq. (8).

$$(8) f = 1 - \max(\text{abs}(\text{MAC}_{ij}))$$

This objective function is used to determine the highest MAC values for identifying the critical modes with similar motions. Next, the MAC repeats the second step by adding one sensor at a time until a required number of sensors are selected. The locations selected for the five accelerometers needed to be installed. It should be noticed that due to the nature of the GA method, the results are usually dependent on the randomly generated initial conditions, which means the algorithm may converge to a different result in the parameter space. These values are very close to the optimal value.

### 7-2- EMAC algorithm

To overcome the contra-decreasing problem of the original MAC algorithm, a forward-backward combinational extension was developed as follows by Li [8]. An EMAC algorithm was proposed to overcome the disadvantages of traditional MAC algorithm with the introduction of a forward-backward combinational approach. First, an intuition sensor set,  $U_0$  (including, to say, a number of sensors,  $s_0$ ) is chosen. Then, one sensor is added to this initial set until a preset number of sensors, which is somewhat larger than the number of sensors as required, for instance, ten percent more than required ( $1.1 s_0$ ), is reached. This is the same as the forward sequential MAC procedure. The extension differs from the original forward approach in the stopping criterion. The EMAC algorithm is continued to obtain a sensor set,  $U_1$ , consisting a certain number of sensors (to say,  $s_1$ ,  $s_1 \leq 1.1 s_0$ ) larger than the required one,  $s_0$ , where the original stops.

Secondly, one sensor at each step is excluded from the sensor set  $U_1$  until the required number of sensors  $s_0$  is reached. This is the backward sequential MAC approach, the essential extension to the forward one.

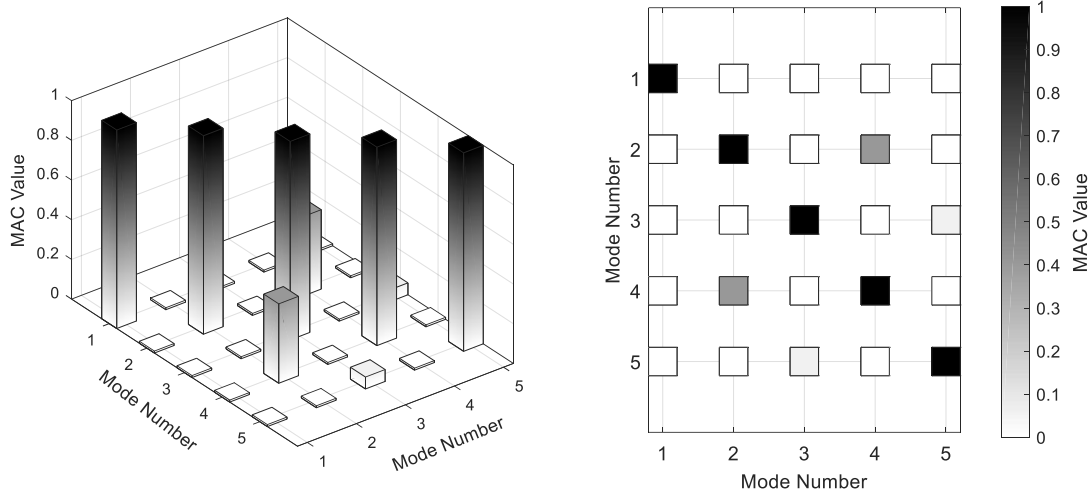
Therefore, two function curves are established. One is the curve of the maximum off-diagonal term with respect to the number of sensors increasing from  $s_0$  to  $s_1$ , which is obtained in the first stage, and the other is the curve of the maximum off-diagonal term with respect to the number of sensors decreasing from  $s_1$  to  $s_0$ , which is found in the second stage. Both curves are compared and the one with a smaller value at the point  $s_0$  is selected. Which curve is to be selected, depends on the abilities of the forward and backward approaches to minimize the maximum off-diagonal terms of the MAC matrix. In this manner, the maximum off-diagonal term of the MAC matrix may, in many instances, be further minimized than the traditional MAC algorithm. Naturally, the forward stopping number of sensors  $s_1$  in the first step can be varied according to the structure under consideration. The effects of various numbers  $s_1$  of sensors on the selection set (including  $s$  sensors) of the above two step processes can be compared and the one with the smallest maximum off-diagonal term of the MAC matrix can be chosen. This can be implemented as the third step, if necessary. There is one note about the influence of the choice of the intuition sensor set,  $U_0$ , on the final selection of sensor positions. If a newly added sensor conflicts with one or several of the original intuition set, the intuition set may be reformed if the exclusion of certain sensor from the original intuition set  $U_0$  is not considered to be much detrimental to the mode shape visualization. Afterwards, the two steps can be recomputed. Tables 5 and 6 demonstrate the values assigned to reproduction parameters and the attained fitness values for MAC and EMAC algorithms. Figure 7 illustrates the MAC matrixes of reduced sensor locations based on MAC and EMAC algorithms.

**Table 5. The values of GA parameters (MAC)**

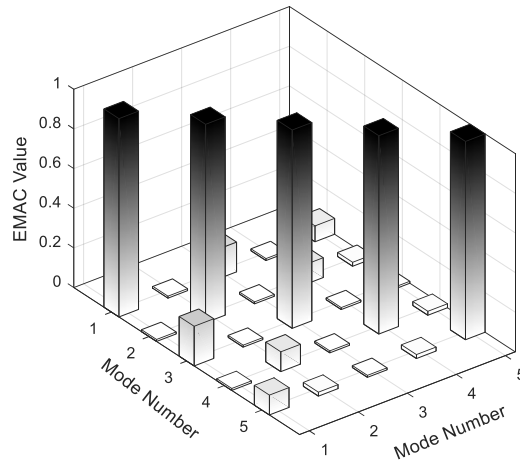
Population	Elite individuals	Crossover individuals	Mutation individuals	Fitness value
100	31	50	22	1.08

**Table 6. The values of GA parameters (EMAC)**

Population	Elite individuals	Crossover individuals	Mutation individuals	Fitness value
100	36	50	27	1.31



(a)



(b)

**Fig. 7. The MAC matrix of reduced sensor locations based on a) MAC b) EMAC algorithms**

### 7-3- TTFD (modified MAC) algorithm

Any signal can completely be described in time or frequency domain, and so, the equivalent periods  $T_{ei}$  are obtained [44]. Both representation data in time or frequency domain can transform to each other. These transformation, the so-called Fourier Transformation and the Inverse Fourier Transformation, are given in Equations (9) and (10), respectively.

$$U(\omega) = \int_{-\infty}^{+\infty} u(t) \cdot e^{-i\omega t} dt \quad (9)$$

$$u(t) = \frac{1}{2\pi} \int_{-\infty}^{+\infty} U(\omega) \cdot e^{i\omega t} d\omega \quad (10)$$

There was no precisely dynamic response on the past presented OSP algorithms, and the authors of this article developed the TTFD algorithm on the basis of NTA. The mathematical process of TTFD is given by

Eq. (11). In first step of this approach, the results of the non-linear analysis were used in order to obtain the exact sensors placement. The values of displacement-time output results in time domain must be transformed to frequency-domain in the second step of this approach based on Eq. (10). In the next step of TTFD approach, the effective frequencies according the maximum Fourier amplitude were selected. In fourth step of this method,

$$t_i = \begin{Bmatrix} t_1 \\ t_2 \\ t_3 \\ \vdots \\ t_n \end{Bmatrix} \xrightarrow{\text{Step1}} u(t)_i = \begin{Bmatrix} u(t)_1 \\ u(t)_2 \\ u(t)_3 \\ \vdots \\ u(t)_n \end{Bmatrix} \xrightarrow{\text{Step2}} U(\omega)_i = \begin{Bmatrix} U(\omega)_1 \\ U(\omega)_2 \\ U(\omega)_3 \\ \vdots \\ U(\omega)_n \end{Bmatrix} \xrightarrow{\text{Step3}} f_{ei} = \begin{Bmatrix} f_{e1} \\ f_{e2} \\ f_{e3} \\ \vdots \\ f_{en} \end{Bmatrix} \Rightarrow T_{ei} = \begin{Bmatrix} T_{e1} \\ T_{e2} \\ T_{e3} \\ \vdots \\ T_{en} \end{Bmatrix}$$

(11)

$$T_{ei} = \begin{Bmatrix} T_{e1} \\ T_{e2} \\ T_{e3} \\ \vdots \\ T_{nen} \end{Bmatrix} \xrightarrow{\text{Step4}} u(z)_{ei} = \begin{Bmatrix} u_{j(z)e1} \quad j=1 \rightarrow n \\ u_{j(z)e2} \quad j=1 \rightarrow n \\ u_{j(z)e3} \quad j=1 \rightarrow n \\ \vdots \\ u_{j(z)nen} \quad j=1 \rightarrow n \end{Bmatrix} \quad \& \quad u(x)_{ei} = \begin{Bmatrix} u_{j(x)e1} \quad j=1 \rightarrow n \\ u_{j(x)e2} \quad j=1 \rightarrow n \\ u_{j(x)e3} \quad j=1 \rightarrow n \\ \vdots \\ u_{j(x)nen} \quad j=1 \rightarrow n \end{Bmatrix} \xrightarrow{\text{Step5}} \text{ModifiedMAC}$$

In this study, a novel approach of OSP algorithms with combination between MAC and TTFD were utilized. The CQC method was utilized as a famous modal combination technique. However, after the time frequency transformation, the corresponded values of time history analysis should be substituted with the MA outcomes. Hence, all of the required parameter values in the CQC such as

the normalized seismic displacement of each effective period was considered. In this respect, these normalized displacement in  $Z$  ( $j=1:n$ ) direction act as mode shape in MAC analysis. In this equation,  $n$  is the number of levels of dam considered to install the fiber Bragg grating (FBG) sensors. The modified type of MAC values can be obtained from MAC in the last step of this approach.

maximum modal responses are replaced with transformed equivalent time histories results. As sample of carried out analysis, Figure 8 illustrates the response acceleration-time diagram of Landers earthquake (1992) and corresponded time-frequency domain transformation.

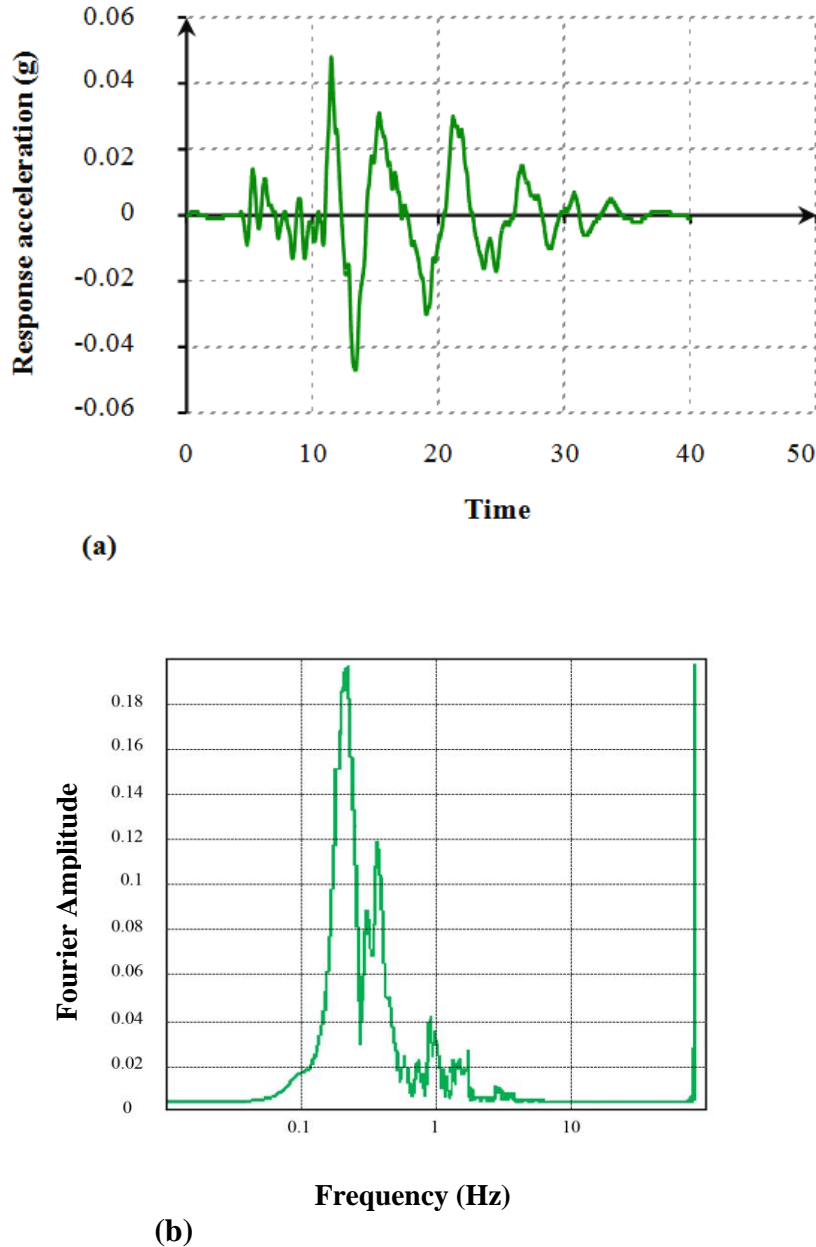


**Fig. 8. (a) Response acceleration-time diagram of Landers earthquake (1992) and (b) corresponded time-frequency domain transformation**

According to ASCE code [45], since maximum modal responses do not occur for different modes in an impact wave simultaneously, therefore, maximum modal responses in different members of a structure via a statistical method should be estimated. The mentioned statistical method should be as indicated by the maximum displacements of different modes and it should include the effects of probable interactions between different displacements close together that are derived from different modes. The peak value

of the total response  $U$  is estimated by combining the peak modal response of individual modes using the modified double sum equation as given by Eq. (12) [46]:

$$F_i = \max \left[ \left( \sum_{i=0}^{h/t} G(x_1) \right) + \left( \sum_{h/t}^{2h/t} G(x_2) \right) + \dots + \left( \sum_{(t-1)h/t}^h G(x_u) \right) \right] \quad (12)$$

$$\text{where: } G(x_u) = U^2 = \sum_{n=1}^N U_n^2 + 2 \sum_{n=1}^{N-1} U_n^2 \sum_{m=n+1}^N \rho_{nm} U_n U_m$$

In Eq. (12),  $F_i$  is the fitness function,  $t$  is the section number,  $h$  is the maximum structure height,  $U_n$  is the maximum modal response in the  $n$ th mode, and  $\rho_{nm}$  is the modified correlation factor defined as:

$$\rho_{nm} = \alpha_n \alpha_m + \sqrt{((1 - \alpha_n^2)(1 - \alpha_m^2))} \rho_{nm} \quad (13)$$

where  $\alpha_n$  is the rigid response coefficient in the  $n$ th mode and  $\rho_{nm}$  is the correlation coefficient of the damped periodic part of modal responses, given by the well-known CQC rule. For damped periodic modes,  $\alpha = 0$ , and modified double sum equation reduces to CQC and for  $\rho_{nm} = 0$ , modified double sum method reduces this to the SRSS. Equations (12) and (13) include the effect of rigid response of high frequency modes in the modified correlation coefficient  $\rho_{nm}$ . The rigid response coefficient  $\alpha_n$  is defined as [47]:

$$\alpha_n = -\frac{\int_0^{t_d} \ddot{x}_n(t) \ddot{u}_g(t) dt}{t_d \sigma_n^{\ddot{x}} \sigma^{\ddot{u}_g}} \quad (14)$$

where  $\ddot{x}_n(t)$  is the acceleration response,  $\sigma_n^{\ddot{x}}$  and  $\sigma^{\ddot{u}_g}$  are the standard deviations of  $\ddot{x}_n(t)$  and  $\ddot{u}_g(t)$ , respectively, and  $t_d$  is the duration of responses. The modal responses, having a frequency less than rigid frequency, have a rigid content, and the value of  $\alpha$  gradually reduces from 1 to zero from a key frequency  $f_2$  to another key frequency  $f_1$  [46]. The key frequency  $f_2$  is the lowest frequency at which the rigid response coefficient becomes 1 and the key frequency  $f_1$  is the highest frequency at which the rigid response coefficient becomes zero. An approximate equation for  $\alpha_n$  can be represented by a straight line between the two key frequencies  $f_1$  and  $f_2$  on a semi logarithmic graph, which is given by Eq. (15) [46]:

$$\alpha_n = \frac{\ln \frac{f_n}{f_1}}{\ln \frac{f_2}{f_1}} \quad 0 \leq \alpha_n \leq 1 \quad (15)$$

where  $f_n$  is the modal frequency (Hz) and the key frequencies  $f_1$  and  $f_2$  can be expressed as,

$$f_1 = \frac{(S_A)_{\max}}{2\pi(S_V)_{\max}} \quad (16)$$

$$f_2 = \frac{(f_1 + 2f^r)}{3} \quad (17)$$

where  $(S_A)_{\max}$  = maximum spectral acceleration,  $(S_V)_{\max}$  = maximum spectral velocity and  $f^r$  = rigid frequency.

In this study, the number of variables is equal to 6, and 18 constraints have been considered. The sections number is equal to seven. It implies that the height of the structure is 21.0 m, and therefore the length of each section is found to be 3.0 m. At the first,  $\rho_{nm}$  was calculated then the square of total response  $G(x_u)$  was computed using  $\rho_{nm}$ ,  $U_n$  and  $U_m$  parameters. Each of the variables should be less than the maximum modal response corresponding to that mode in the each section. Eq. (12) was employed as the fitness function in this framework. This function was maximized by the GA system in the process of evolutionary optimization. When performing the OSP method via the GA technique, certain parameters are required such as constraints, fitness function, population size, elite individuals, crossover method, crossover individuals, mutation individuals, and fitness value. Table 7 demonstrates the values of GA parameters. Figure 9 clearly shows the evolution process of best fitness values of GA according to TTFD method. Finally, after obtaining  $G(x_u)$  values using the optimization process, the Lagrangian interpolation was undertaken in each section considering the initial results of the square of total response, due to finding the optimal locations in each section.

According to this optimization method and considering the GA results, the best sensor locations in the BI building are presented as the final results in Table 8-10.

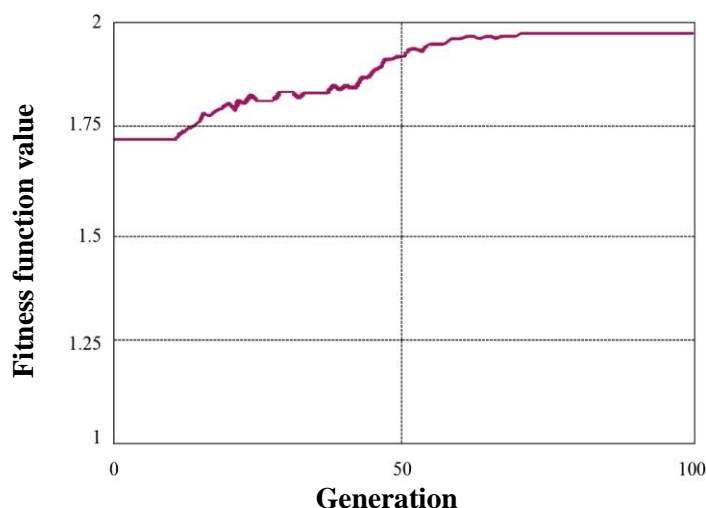


**Fig. 9.** The evolution progress of the best fitness value of GA according to TTFD method

**Table 7.** The values of GA parameters (TTFD)

Population	Elite individuals	Crossover individuals	Mutation individuals	Fitness value
100	39	50	32	1.98

**Table 8.** Details of OSP by GA in the seven sections using TTFD approach (Landers-1992)

Stage	1 (0-3.0 m)	2 (3.01-6.0 m)	3 (6.01-9.0 m)	4 (9.01-12.0 m)	5 (12.01-15.0 m)	6 (15.01-18.0 m)	7 (18.01-21.0 m)
X direction (m)	1.98	4.28	7.79	10.08	13.12	16.47	19.88
Y direction (m)	1.12	3.92	7.16	9.86	12.74	16.04	19.33
Z direction (m)	1.39	4.09	7.39	10.01	12.96	16.19	19.57

**Table 9.** Details of OSP by GA in the seven sections using TTFD approach (San Fernando-1971)

Stage	1 (0-3.0 m)	2 (3.01-6.0 m)	3 (6.01-9.0 m)	4 (9.01-12.0 m)	5 (12.01-15.0 m)	6 (15.01-18.0 m)	7 (18.01-21.0 m)
X direction (m)	1.54	3.76	7.31	9.73	12.86	15.95	19.47
Y direction (m)	0.96	3.57	6.92	9.29	12.43	15.71	18.92
Z direction (m)	1.21	3.63	7.17	9.58	12.64	15.83	19.28

**Table 10.** Details of OSP by GA in the seven sections using TTFD approach (Northridge-1994)

Stage	1 (0-3.0 m)	2 (3.01-6.0 m)	3 (6.01-9.0 m)	4 (9.01-12.0 m)	5 (12.01-15.0 m)	6 (15.01-18.0 m)	7 (18.01-21.0 m)
-------	-------------------	----------------------	----------------------	-----------------------	------------------------	------------------------	------------------------



X direction (m)	1.76	3.97	7.46	9.87	12.94	16.12	19.51
Y direction (m)	1.04	3.69	7.01	9.42	12.52	15.85	19.08
Z direction (m)	1.28	3.86	7.22	9.78	12.81	15.96	19.34

## 8. Conclusion

In this paper, three reliable methods for OSP of a BI building, based on modal and NTA results have been utilized. Real-coded elitist GAs with uniform parent centric crossover operators and mutation operators were developed and used for the implementation of the OSP process.

Three different strategies, including MAC, EMAC, and TTFD were investigated for OSP in a 5-story BI building. The MAC algorithm is a basic OSP method whereas EMAC is a new algorithm containing the improved MAC and they utilize the free vibration analysis results on OSP process. In the following, a novel OSP approach was proposed by authors that was named TTFD algorithm. The mentioned approach uses NTA results as an exact seismic response; however, the MAC and EMAC algorithms utilize the modal analysis results. As a comparison, the OSP results revealed since the TTFD employs the accurate data (seismic response) as input, this led to acquiring the sensor locations with a high precision rate.

## 8. References

- [1]. Wang, J., Lin, C., and Min Yen, S. (2007). A story damage index of seismically-excited buildings based on modal frequency and mode shape, *Engineering Structures*, 29(9), 2143-2157.
- [2]. Allemang, R.J., and Brown, D.L. (1982). A correlation coefficient for modal vector analysis, In: *Proceedings of the international modal analysis conference*, 110-116, <https://www.semanticscholar.org/paper/A-Correlation-Coefficient-for-Modal-Vector-Analysis-Allemang-Brown/5b38c729b278f8af61491f6a643912c185783cc8>.
- [3]. Ewins, D.J. (1984). *Modal testing: Theory and practice* (Dewey Number: 624.1/71), London: Research Studies Press Ltd.
- [4]. Lieven, N.A.J., and Ewins, D.J. (1988). Spatial correlation of mode shapes, the coordinate modal assurance criterion (COMAC), In: *Proceedings of the sixth international modal analysis conference*, vol. II, Hyatt, OR, Union College, 690-695.
- [5]. Ndambi, J-M., Vantomme, J., and Harri, K. (2002). Damage assessment in reinforced concrete beams using eigenfrequencies and mode shapes derivatives, *Engineering Structures*, 24, 501-515.
- [6]. Brasiliano, A., Doz, G.N., and Brito, J.L.V. (2004). Damage identification in continuous beams and frame structures using the residual error method in the movement equation, *Nuclear Engineering and Design*, 227, 1-17.
- [7]. Carne, T. G., and Dohrmann, C. R. (1994). A modal test design strategy for model correlation (Report Number: Conf-950240-4), In: *international modal analysis conference*, Nashville, TN, 927-933, <http://adsabs.harvard.edu/abs/1995SPIE.2460.927C>.
- [8]. Li, D. (2011). *Sensor placement methods and evaluation criteria in structural*

- health monitoring*, Ph. D. thesis, University of Siegen, Siegen.
- [9]. Kammer, D.C. (1991). Sensor placement for on-orbit modal identification and correlation of large space structures, *Journal of Guidance, Control, and Dynamics (AIAA)*, 14(2), 251-259.
- [10]. Kammer, D.C. (1992). Effect of model error on sensor placement for on-orbit modal identification of large space structures, *Journal of Guidance, Control, and Dynamics (AIAA)*, 15 (2), 334-341.
- [11]. Imamovic, N. (1998). *Validation of large structural dynamics models using modal test data*, Ph. D. thesis, Imperial College of Science, Technology & Medicine. London.
- [12]. International, L. (1991). Large-scale modal testing of a space frame structure-from pretest analysis to FEA model validation, *Journal of Sound and Vibration*, 10, 6-16.
- [13]. Heo, G., Wang, M.L., and Satpathi, D. (1997). Optimal transducer placement for health monitoring of long span bridge, *Soil Dynamics and Earthquake Engineering*, 16 (7-8), 495-502.
- [14]. De Clack, L.P., and Avitabile, P. (1996). Development of several new tools for modal pre-test evaluation, In: *Proceedings of the 14<sup>th</sup> international modal analysis conference*, Dearborn, 1272-7, <https://www.semanticscholar.org/paper/Development-of-Several-New-Tools-for-Modal-Pre-test-Declerck-Avitabile/23dafb143a8b709e1b84bd4def528b59cda0e0cb>.
- [15]. Kienay, D., Richrrrdson, M., and Blakely, K. (1989). Using finite element data to set up modal tests, *Journal of Sound and Vibration*, 23, 16-23.
- [16]. Papadimitriou, C. (2004). Optimal sensor placement methodology for parametric identification for structural systems, *Journal of Sound and Vibration*, 278 (4), 923-947.
- [17]. Papadimitriou, C. (2005). Pareto optimal sensor placement locations for structural identification, *Journal of Computer Methods in Applied Mechanics and Engineering*, 194 (12), 1655-1673.
- [18]. Limongelli, M. P. (2003). Optimal location of sensors for reconstruction of seismic responses through spline function interpolation, *Journal of Earthquake Engineering Structure Dynamics*, 32, 1055-1074.
- [19]. American Institute of Steel Construction (AISC) (2016), in *Manual of Steel Construction-Load Resistance Factor Design*, Chicago, AISC.
- [20]. Ahmadi, S.L. and Tadjbakhsh, I.G. (1989). A comparative study of performances of various base isolation systems, Part 1: Shear beam structures, *Journal of Earthquake Engineering Structure Dynamics*, 18, 11-32.
- [21]. Chen, C., Yeh, K., and Liu, F. (2009). Adaptive fuzzy sliding model control for seismically excited bridges with lead rubber bearing isolation, *International Journal of Uncertainty Fuzziness and Knowledge-Based Systems*, 17 (5), 705–727.
- [22]. Lee-Glauser, G.J., Ahmadi, G., and Horta, L.G. (1997). Integrated passive/active vibration absorber for multistory buildings, *ASCE Journal of Structural Engineering*, 123, 499-504.
- [23]. Su, L., Ahmadi, G., and Tadjbakhsh, I.G. (1989). Comparative study of base isolation systems, *ASCE Journal Engineering Mechanics*, 115, 1976-1992.

- [24]. Robinson, W.H. (1982). Lead-rubber hysteretic bearings suitable for protecting structures during earthquakes, *Journal of Earthquake Engineering Structure Dynamics*, 10, 593-604.
- [25]. Soong, T.T., and Spencer, B.F. (2002). Supplemental energy dissipation: State-of-the-art and state-of-the-practice, *Journal of Engineering Structures*, 24, 243-259.
- [26]. Saiful islam, A.B.M., Rizwan hussain, R., jumaat, M., and Rahman, M.A. (2013). Nonlinear dynamically automated excursions for rubber-steel bearing isolation in multi-storey construction, *Journal of Automation in construction*, 30, 265-275.
- [27]. Uniform Building Code (UBC) (1997). *International conference of building officials*, Whittier, CA: UBC.
- [28]. Jangid, R.S., and Kelly, J.M. (2001). Base isolation for near-fault motions, *Journal of Earthquake Engineering Structure Dynamics*, 30, 691-707.
- [29]. Rodriguez-Marek, A. (2000). *Near fault seismic site response*, Ph.D. Thesis, Civil Engineering, University of California, Berkeley, CA, USA.
- [30]. Providakis, C.P. (2008). Effect of LRB isolators and supplemental viscous dampers on seismic isolated buildings under near-fault excitations, *Journal of Engineering Structures*, 30 (5), 1187-1198.
- [31]. Baker, J.W. (2007). Quantitative classification of near-fault ground motions using wavelet analysis, *Bulletin of the Seismological Society of America*, 97, 1486-1501.
- [32]. Mazza, F., and Vulcano, A. (2009). Nonlinear response of RC framed buildings with isolation and supplemental damping at the base subjected to near-fault earthquakes, *Journal of Earthquake Engineering*, 13, 690-715.
- [33]. Mazza, F., Vulcano, A., and Mazza, M. (2012). Nonlinear dynamic response of RC buildings with different baseisolation systems subjected to horizontal and vertical components of near-fault ground motions, *The Open Construction and Building Technology Journal*, 6, 373-383.
- [34]. Hu, J.W., and Leon, R.T. (2011). Analysis and evaluations for composite-moment frames with SMA PR-CFT connections, *Nonlinear Dynamics*, 65, 433-455.
- [35]. Hu, J.W., Choi, E., and Leon, R.T. (2011). Design, analysis, and application of innovative composite PR connections between steel beams and CFT columns, *Smart Materials and Structures*, 20(2), 1-15.
- [36]. Jangid, R.S. (2007). Optimum lead-rubber isolation bearings for near-fault motions, *Journal of Engineering Structures*, 29, 2503-2513.
- [37]. Hu, J.W., Kang, Y.S., Choi, D.H., and Park, T. (2010). Seismic design, performance, and behavior of composite-moment frames with steel beam-to-concrete filled tube column connections, *International Journal of Steel Structures*, 10, 177-191.
- [38]. Hwang CL. and Yoon, K. (1981). Methods for Multiple Attribute Decision Making, *Multiple Attribute Decision Making*, 58-191.
- [39]. Goldberg, D. E. (1989). *Genetic Algorithms in Search, optimization and machine learning*, Addison-Wesley Pub. Co., Reading, Mass., xiii, 412 pages.
- [40]. Tongpadungrod, P., Rhys, T. D. L. and Brett, P. N. (2003). An approach to

optimise the critical sensor locations in one-dimensional novel distributive tactile surface to maximize performance, *Journal of Sensors and Actuators*, 105, 47-54.

- [41]. Huang, W. P., Liu, J., and Li, H. J. (2005). Optimal sensor placement based on genetic algorithms, *Journal of Engineering Mechanics*, 22(1), 113-117.
- [42]. Guo, H. Y., Zhang, L., Zhang, L. L. and Zhou, J. X. (2004). Optimal placement of sensors for structural health monitoring using improved genetic algorithms, *Journal of Smart Materials and Structures*, 13, 528-534.
- [43]. Yi, T. H., Li, H. N. and Gu, M. (2011). Optimal sensor placement for health monitoring of high-rise structure based on genetic algorithm, *Journal of Mathematical Problems in Engineering*, 11.
- [44]. Sadat Shokouhi, S.K., and Vosoughifar, H.R. (2013). Optimal sensor placement in the lightweight steel framing structures using the novel TTFD approach subjected to near-fault earthquakes, *Journal of Civil Structural Health Monitoring*, 3 (4), 257-267.
- [45]. ASCE standard code (2005). *Minimum design loads for buildings and other structures*, ASCE, USA.
- [46]. Gupta, A. K., Hassan, T. and Gupta, A. (1996). Correlation coefficients for modal response combination of non-classically damped systems, *Journal of Nuclear Engineering and Design*, 165, 67-80.
- [47]. Dong, C. (1998). Generalized genetic algorithm, *Journal of Exploration of Nature*, 63(17), 33-37.